# Graphene-Based Conformal Devices

**Yong Ju Park,[†,⊥] Seoung-Ki Lee,[†,⊥] Min-Seok Kim,[‡] Hyunmin Kim,[§] and Jong-Hyun Ahn[†,*]**

[†]School of Electrical and Electronic Engineering, Yonsei University, Seoul 120-749, Korea, [‡]Center for Mass Related Quantities, Korea Research Institute of Standards and Science, Daejeon 305-340, Korea, and [§]Nano & Bio Research Division, Daegu Gyeongbuk Institute of Science and Technology, Daegu 711-873, Korea. [⊥]Yong Ju Park and Seoung-Ki Lee contributed equally to this work.

**ABSTRACT** Despite recent progress in bendable and stretchable thin-film transistors using novel designs and materials, the development of conformal devices remains limited by the insufficient flexibility of devices. Here, we demonstrate the fabrication of graphene-based conformal and stretchable devices such as transistor and tactile sensor on a substrate with a convoluted surface by scaling down the device thickness. The 70 nm thick graphene-based conformal devices displayed a much lower bending stiffness than reported previously. The demonstrated devices provided excellent conformal coverage over an uneven animal hide surface without the need for an adhesive. In addition, the ultrathin graphene devices formed on the three-dimensionally curved animal hide exhibited stable electrical characteristics, even under repetitive bending and twisting. The advanced performance and flexibility demonstrated here show promise for the development and adoption of wearable electronics in a wide range of future applications.

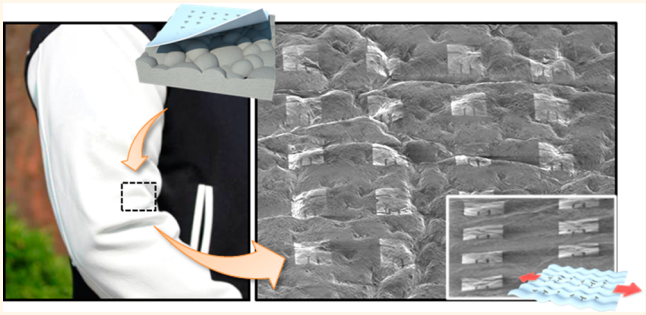

**KEYWORDS:** ultrathin transistor · tactile sensor · graphene · conformal device · wearable electronics

Recently, conformal devices on uneven surface have garnered great popularity due to their multifaceted applications in healthcare monitoring systems[1−3] and wearable electronics.[4] Such devices are hardly achievable using a sophisticated planar layout; rather, the fabrication of them strictly requires a new design of device geometry and a relevant adopt of materials that can compensate structural imperfections. Thus, most of the current research has been focusing on how to maximize the structural compliance of "implanted" devices with regards to the environment; strain is regarded as one of the major critical challenges to overcome, the solution of which is not fully provided yet, especially as for the mechano-compatibility of the devices with respect to *in vivo* circumstances.

Strain, which can seriously degrade device performance, is locally generated and distributed across the device in a physical contact with a rough surface. In an effort to address this issue, various approaches have been developed. The representative methods have been used by employing elastic conductors composed of elastic rubbers and conductive materials such as micrometer-sized silver flakes, metal wires and carbon nanotubes.[5−7] Net-shaped and fractured metallic film has also been demonstrated as a solution that can absorb any strain by bending/flexing of the devices.[8−10] Although these approaches are potentially useful in three-dimensional electronics systems, its application is restricted to the objects with simple curvatures. Another approach for conformal devices involves interconnecting a series of rigid active devices with "shock-absorbing" bridges that can accommodate both compressive and tensile stresses.[11−15] This method has been exemplified in a course of applications, including electronic eye cameras,[16] stretchable transistors,[17] and flexible solar cells.[18] Unfortunately, various additional processes must be accompanied to achieve intended results in this case. Prestraining or premolding substrate can limit the range of available applications. Indeed, the delicate tolerance to the collision and friction stemming from out-of-plane buckling of the interconnector becomes a significant hurdle for this method. Recently, epidermal electronics based on the combination of ultrathin silicon membrane with filamentary serpentine metal mesh have been extensively exploited; some applications of these systems are medical sensors to monitor body temperature[3] and neural/electrophysiological signals.[2,4,19] Although there are considerable advantages with established silicon

* Address correspondence to ahnj@yonsei.ac.kr.

Received for review June 25, 2014 and accepted July 29, 2014.

**Published online July 29, 2014**
**10.1021/nn503446f**

technology in the device design, the silicon-membrane-based devices still have a critical drawback in bending inflexibility even when assembled with the soft substrate because the active layer is several hundred nanometers thick. A smaller bending "stiffness" would be desired to achieve an enough conformal coverage over the uneven "wrinkle-prone" substrate, such as the human skin. Also, the silicon membrane requires an encapsulation layer to obtain conformal attachment to a substrate for stable operation during macroscopic movements of the joints in the human body (*i.e.*, wrist, knee, and elbow), becoming an additional source for the bending stiffness increase.[20] In this light, graphene is an ideal constituent for conformal devices because it is a one-atomic-thick platform with extraordinary mechanical flexibility and optical transmittance.[21,22] A few recent studies have reported the preparation of graphene- or carbon-based flexible field effect transistors on unconventional substrates;[23,24] however, it still remains a significant challenge to integrate the graphene devices on rough substrate such as human skin or animal hide without degradation of electrical characteristics.

In this work, we report the graphene-based devices that can be attached conformably to highly deformed surface such as an animal hide and exhibit stable electrical and mechanical performances under serious external deformations, such as flexion and distortion. With direct application of a polymer film used as a gate dielectric and as a supporting layer of device, the thickness of graphene transistor can be reduced less than 70 nm. Consequently, the demonstrated graphene-based conformal device produced a bending stiffness ($EI$ ~1.24 GPa·$\mu$m$^4$) that was much lower than the values in the literature, leading to an excellent adaptational coverage over uneven surfaces without necessity of an adhesive layer. Furthermore, we demonstrate a tactile sensor-array composed of monolithically patterned graphene film, showing good sensitivity against external force.

## RESULTS AND DISCUSSION

Reducing the device thickness is one strategy for realizing conformal devices because the bending stiffness is proportional to the cube of the thickness.[25] Considerable efforts have been applied toward thinning the device supporting layer since the supporting layer contributes majority of the device thickness and degrades the flexibility of the system.[26] To this end, we designed the fabrication of a stand-alone device prepared without a substrate by substituting a constituent layer that comprises the transistors for the supporting layer. This device structure could be achieved because the graphene layer used as both channel and electrodes was thin, light, and tough, and it did not require an additional supporting layer.

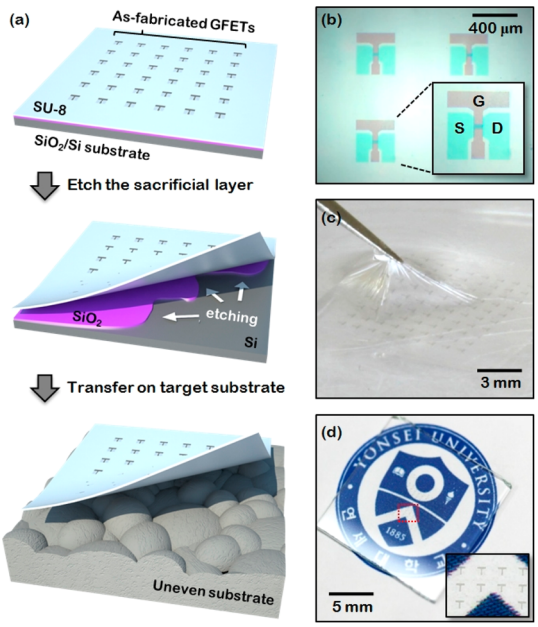


**Figure 1. (a) Schematic diagram showing the procedure used to fabricate array of ultrathin graphene field effect transistors (UT-GFETs). (b) Microscopy image of the as-fabricated UT-GFETs. The gray regions indicate the gate electrode, and the green regions indicate the channels and source/drain electrodes. (c) Optical image of the UT-GFETs floating on DI water during the transfer process. (d) Optical image of the transferred UT-GFETs on a glass substrate.**

Figure 1(a−d) shows schematic diagrams of the entire process for fabricating ultrathin graphene field effect transistors (UT-GFETs) and the optical images of device at each step. First, few-layer graphene (FLG) was synthesized on a Ni catalyst using chemical vapor deposition (CVD). The FLG was then transferred onto a $SiO_2$/Si substrate.[27] The gate electrode was defined using conventional photolithography and oxygen plasma etching processes, as reported previously.[22] After removing the photoresist, SU-8 epoxy, which functioned as both gate dielectric and supporting layer for GFET,[28] was spin-coated onto the device, cross-linked by UV irradiation, and hard-baked. The thickness of the epoxy film was tuned from 70 to 1400 nm by using different volumetric ratios of the epoxy and epoxy thinner. Because the graphene thickness was subnanometer in scale, the total thickness of the GFET device could be regulated by controlling the thickness of the SU-8 epoxy layer. The UT-GFETs were completed by patterning the source (S)/drain (D) electrodes and semiconducting channel region, after transferring the single layer graphene (SLG) grown on Cu foil onto an epoxy coated device.[29,30] The detailed fabrication step was described in Supporting Information. The fabricated UT-GFETs on the $SiO_2$/Si handling substrate had a channel width of 25 $\mu$m and length of 30 $\mu$m, as shown in Figure 1(b). The UT-GFETs were then floated on the surface of a dilute HF solution (HF:DI water =1:10) at room temperature to etch away the $SiO_2$ sacrificial layer.[31] In this step, the epoxy dielectric film acted as a

supporting layer to protect the device from destruction during the transfer process. Thus, we avoided additional spin-coating steps that would require conventional transfer steps in an effort to simplify the fabrication process.[32] Complete removal of the sacrificial layer released the UT-GFETs from the handling substrate, and the UT-GFETs freely floated on the surface of the etchant. The UT-GFETs were rinsed with DI water to remove remaining etchant and were transferred to the target substrate. The outstanding flexibility of the device due to the extreme thinness of the device may be appreciated from the photographic image of the floated UT-GFET film shown in Figure 1(c). The dry transfer method is also described in the Supporting Information. Finally, the devices were transferred to a rough substrate with the help of the capillary forces of water during drying and adhered to the substrate through van der Waals forces alone. Figure 1(d) shows a photograph and magnified image of the UT-GFETs transferred to transparent substrates. As expected, the optical transmittance exceeded 70% across the visible spectrum (Supporting Information, Figure S3). The transmittance was reduced by ~3% in the source (S)/drain (D) electrodes and channel region, and by ~26% at 550 nm in the gate electrode and epoxy dielectric films.

In order to achieve full range of conformal contact between a GFET film and a rugged surface, an adhesive energy was investigated using numerical calculation of two overlapping cylinder models, and the results were compared with experimental measurement as shown in Figure 2. Since the adhesive energy depends strongly on the bending stiffness of a device, a bending stiffness was calculated based on the thickness of the device as well as the mechanical properties of each layer (*i.e.*, Young's modulus and the Poisson's ratio). Figure 2(a) shows the calculated bending stiffness (*EI*) variations of fabricated GFETs as a function of the thickness. The bending stiffness decreased dramatically as the device thickness decreased. At a thickness of 1400 nm, the *EI* was calculated to be 9192.4 GPa·$\mu$m$^4$. This value decreases to 266.35, 36.16, and 1.15 GPa·$\mu$m$^4$ as the GFET becomes thinner to 430, 220, and 70 nm, respectively. Experimentally measured *EI* as marked by red symbols was well matched with the calculated *EI* (Supporting Information, Figure S4). The thinnest GFET among the various devices with different thickness had a value of 1.24 GPa·$\mu$m$^4$. It is worth noting that an *EI* of 1.24 GPa·$\mu$m$^4$ for the 70 nm thick UT-GFETs is the lowest value yet reported for such devices (Supporting Information, Table S2). Finally, the adhesion energy could be calculated according to the following equation:[1]

$$\gamma \geq \gamma_c' = \frac{EI}{2R^2 b}\{1 + (1+\lambda)R^2/[(1-\lambda)\gamma_0^2]\} \quad (1)$$

where $\gamma$ (10 mJ/m$^2$) is the adhesion energy in the wet state,[1,33] $\gamma_c'$ is the calculated adhesion energy, *EI* is the bending stiffness of the device, *R* is the radius of the cylinders, *b* is the width of the device, $\lambda$ is the wavelength, and $\gamma_0$ is the arc between the two cylinders (Supporting Information, Figure S5). For $\gamma \geq \gamma_c'$ in eq 1, a device may make a full conformal contact with the substrate.[1] More detailed information and the calculation process are described in the Supporting Information. Figure 2(b) shows the calculated and measured adhesion energy in devices having a thickness of less than 100 nm. According to the calculations, the critical thickness ($h_c$) for perfect conformal contact on a rugged substrate was 76 nm. Figure 2(d–f) shows FE-SEM images of devices with different thicknesses ($t_{device}$: 70, 220, and 430 nm) transferred onto uneven substrates. The surface roughness ($R_a$) of the rugged substrate was 41 $\mu$m, measured using a surface profiler.[2] When comparing the surfaces of a bare substrate to the transferred 70 nm thick UT-GFETs, which were thinner than $h_c$, the UT-GFETs were found to make contact deep into the concave features of the surface and to wrap along the curves of the substrate without forming cracks or delaminated regions (Figure 2(c,d)). By contrast, devices thicker than $h_c$ made incomplete contact with substrates, as shown in Figure 2(e,f). In other words, the GFET film was suspended by the

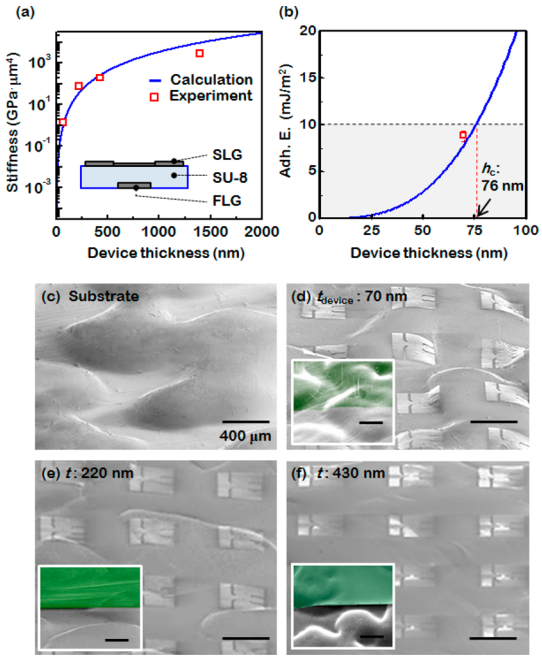


**Figure 2. (a) Calculated stiffness of a UT-GFET prepared with a range of device thickness values. Red square indicate the experimentally measured stiffness values at 70, 220, 430, and 1400 nm, the thicknesses of the fabricated UT-GFET devices. (b) Calculated adhesion energy of the UT-GFET as a function of device thickness. Mechanical modeling revealed that the UT-GFET film could achieve conformal contact in devices <76 nm thick. (c) SEM images of a rugged substrate prior to transferring the UT-GFETs. (d–f) SEM images of the UT-GFETs transferred onto the rugged substrate, for device thickness values of 70, 200, and 430 nm. The inset image shows the magnified edge part of the GFET film. Scale bar, 100 $\mu$m.**

surrounding ridges and generated wrinkles as well as noncontacted region. These differences were scrupulously verified at the edges of the film, as displayed in the inset of Figure 2(d,f).

The extent of conformal coverage attained by scaling down the device thickness influenced the adhesion strength (mainly the van der Waals force) between the GFET film and the substrate.[1,34] If the bonding strength of the GFET film on a substrate is weak, the device can be detached only by weak external forces. Therefore, it was necessary to evaluate the bonding (*i.e.*, adhesion) strength between the device and the substrate.[35−37] Figure 3 shows the results of the adhesion strength tests, as a function of the device thicknesses, measured through a series of pull-off tests using the samples shown in Figure 2. A schematic illustration of the pull-off test is showed in Figure 3(a). A polydimethylsiloxane (PDMS) elastic stamp, which was designed to have a contact area of 0.5 × 0.5 $cm^2$, was mounted on the end of a cantilever and pressed against the transferred GFETs with an applied load of 1 N. After a 5 s dwell time, the PDMS stamp was pulled up from the substrate. The pull-off adhesion strength was recorded when the PDMS stamp had been completely released from the substrate. The real contact area between GFET film and PDMS substrate during the whole process was monitored using a charge-coupled device camera. Figure 3(b) presents plots of the contact area between the GFET film and the substrate, and the pull-off force variations as a function of the device thickness. The defined contact areas analyzed by the software ImageJ were 4.5, 10.9, 23.9, and 97.1% on 1400, 340, 220, and 70 nm thick devices, respectively (Supporting Information, Figure S6). It should be noted here that the contact area increased dramatically as the devices became thinner. This behavior resulted from the relationship between the bending stiffness and the device thickness. The bending stiffness, greatly reduced by the reduced device thickness, dramatically increased the coverage area. Because the contact strength is proportional to the coverage area, the UT-GFETs can adhere strongly to a substrate without the help of an adhesive.[35] At a contact load of 1 N, the pull-off force increases by a factor of nearly 30 (from 2.22 to 68.17 mN) as the thickness is changed from 1400 to 70 nm.

The feasibility of using the fabricated device for realistic applications was tested by applying the UT-GFETs (*t*: 70 nm) onto animal hide and measuring the electrical properties. The inset of Figure 4(a) shows an optical image of the UT-GFETs transferred onto hide using the dry transfer technique illustrated in Figures 1 and S2 (Supporting Information). As-fabricated UT-GFETs on the $SiO_2$/Si substrate were fully transferred onto the target substrate while preserving their original device array. The T-shaped gray region indicates a gate electrode made of FLG. The channel and S/D electrodes composed of SLG were difficult to identify in

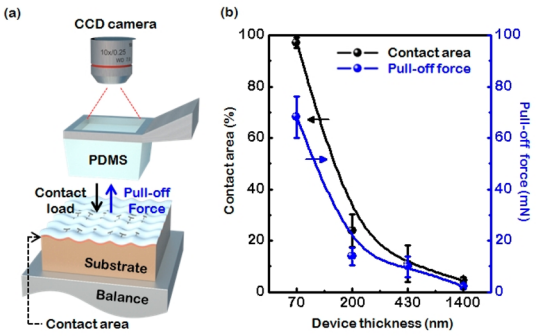


**Figure 3. (a) Schematic illustration of the pull test. The transferred UT-GFETs contacted the PMDS stamp, and the contact region was monitored using a CCD camera. (b) Calculated contact area between the UT-GFETs and the rugged substrate (black line), and the measured pull-off force (blue line) as a function of device thickness.**

the photograph due to their excellent transparency properties. Rigorous inspection by FE-SEM revealed conformal contact between the UT-GFETs and the hide (Figure 4(a)). Interestingly, the UT-GFETs covered the bumpy surface well, even the narrow crevices; however, several fine wrinkles were also found due to the presence of extremely small bumps. Compared with a silicon membrane of the same thickness ($t_{Si}$: ∼ 70 nm), which was studied previously as a potential conformal device, the UT-GFETs array film exhibited better coverage over uneven surfaces because the devices were composed of an atomic-scale graphene layer and a flexible polymer dielectric layer, in contrast with the rigid silicon membrane (Supporting Information, Figure S7).

Prior to measuring the electrical properties of conformal GFETs, the GFETs were categorized as *flat*, *sloped*, and *valley* depending on the position of the channel on the hide. Namely, the channels that have a positive and a negative curvature on the surface were classified into sloped and valley, respectively. It is desirable to quantify the effects of the external strain created from the surface curvature on the electrical characteristics. The representative SEM images of each transistor and the surface profile of the hide was presented in Figure 4(b). Significantly large strain was expected to be applied to the transistor at the valley positions which corresponded to the regions of greatest deformation from a flat conformation. However, although the minimum radius of curvature ($R_c$) in the valley regions was ∼4 $\mu$m, the applied compressive strain on the device was less than 1% due to extremely thin device thickness,[38] which falls in the range of endurable strains for the UT-GFETs.[39] Moreover, because other sloped and flat positions spontaneously formed conformal contact with the substrate during the transfer process without introducing any external stresses, the strain at both the sloped and flat positions approached zero. To get more reliable verification, we performed Raman measurement on graphene.

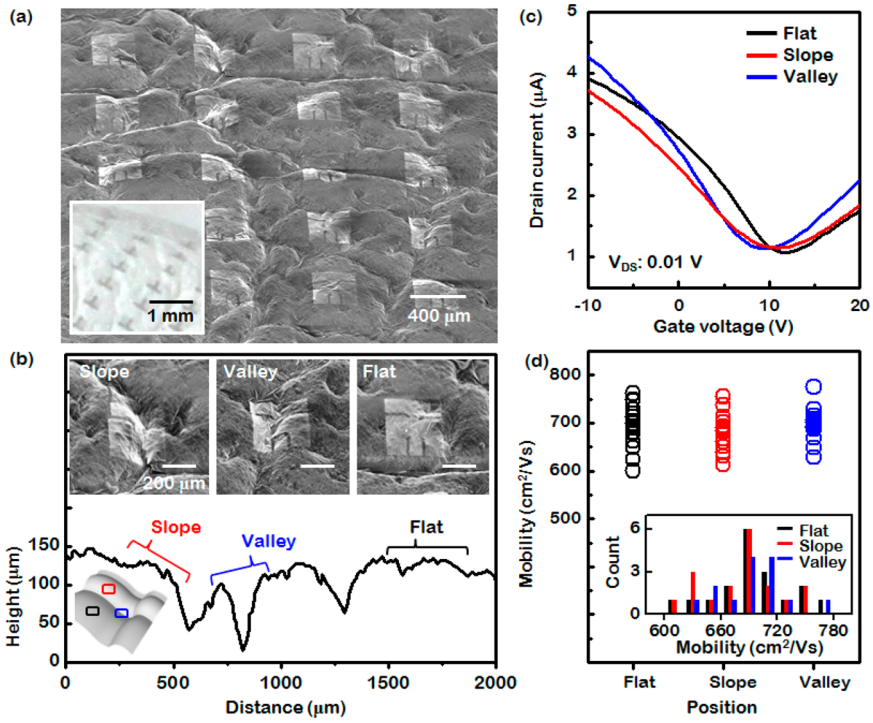


**Figure 4. (a) SEM image of the UT-GFETs mounted on the animal hide substrate. The inset image shows a photograph of the UT-GFETs. (b) Surface profile of the animal hide. Depending on the position of the channel on the hide, the device was classified into 3 categories: flat, sloped, and valley. The inset images show representative SEM images of the UT-GFETs on the flat, sloped, and valley regions. (c) Representative transfer characteristics of the UT-GFETs on flat, sloped, and valley regions. (d) Distribution of hole mobility of UT-GFETs, which are located on the flat, sloped, and valley regions; inset shows the mobility histogram of UT-GFETs on hide.**

As a result, the 2D Raman band corresponding graphene did not reveal any noticeable shifts in each region, indicating that an undetectable level of strain was applied to the graphene (Supporting Information, Figure S8).[40] The transfer characteristics of the devices were subsequently measured from UT-GFETs positioned in different regions of the hide. The drain bias was fixed at 0.01 V and the gate voltage was swept from −10 to 20 V. Since the device configurations are not uniform, statistical analysis of electrical property was carried out from 50 devices. Black, red, and blue lines indicate the representative transfer characteristics of the transistor from flat, sloped, and valley positions, respectively. Interestingly, the transistors exhibited similar electrical characteristics on each location. This indicates that the geometry of hide cannot greatly influence on the electrical transport property of UT-GFETs. It is considered that the thickness of the device with a few tens of nanometers and wet transfer method based on surface tension of water can minimize the stress to the GFET when formed on bumpy substrate.[1,38] Undoubtedly, the robust feature of graphene against external strain plays an indispensable role to realize conformal device. As shown in Figure 4(c,d), the transistors operated uniformly overall, regardless of the location on hide. The calculated average hole and electron mobilities were 695 ± 41 and 379 ± 13, 692 ± 24 and 402 ± 30, and 701 ± 22 and 398 ± 12 $cm^2/V \cdot s$ on the flat, sloped, and valley positions, respectively (Supporting Information, Figure S9). The relatively low mobility of the UT-GFETs may have resulted from the poor interfacial properties of the SU-8 epoxy gate insulator and graphene.

Another notable advantage of the conformal UT-GFETs is their good mechanical stretchability across three-dimensionally curved surfaces. Curved substrates coated with the UT-GFETs could consume the external strain rather than transferring it to the device by transforming and flattening the surface shape. The stretchability of the device was examined by measuring the deformations of the UT-GFETs using SEM (Figure 5(a)). As the substrate was stretched up to 4%, the uneven surface gradually flattened, and only fine vertical wrinkles were generated due to the Poisson effects. Consequently, the GFETs remained stable under external stretching without compromising the physical integrity of the device, as has been observed in wavy structured devices.[12,13] However, the device located on valley region was preferentially delaminated from the hide at serious stretching because relatively large deformation occurred first in a valley region. This failure can be controlled by improving an adhesion between a device and a substrate. The practical feasibility of using conformal UT-GFETs as wearable electronics was demonstrated by monitoring the electrical characteristic of a substrate during folding and twisting, which are the

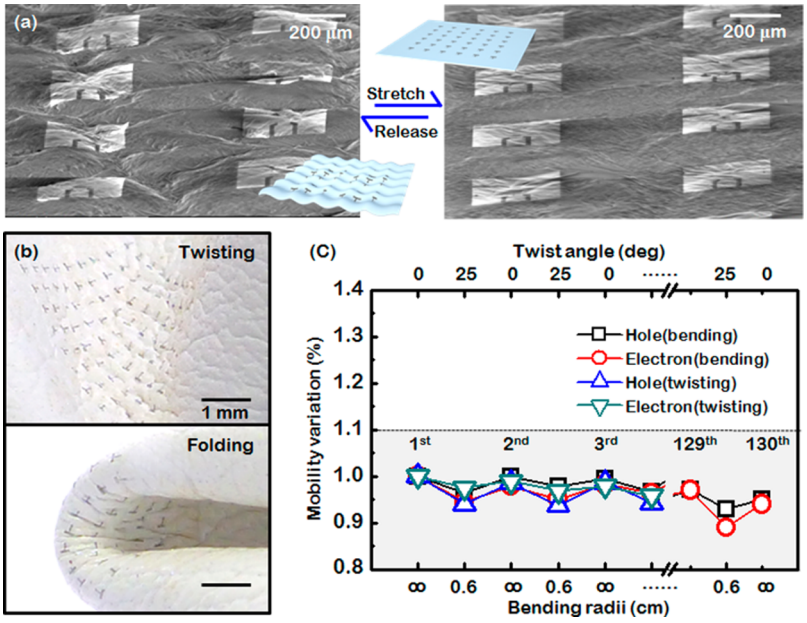


**Figure 5. (a) SEM images of the UT-GFETs released onto the hide (left) or mechanically stretched under a 5% extension (right). (b) Photographs of the twisted and folded UT-GFETs mounted on the animal hide substrate. (c) Mobility measurements during repeated deformations of the substrate.**

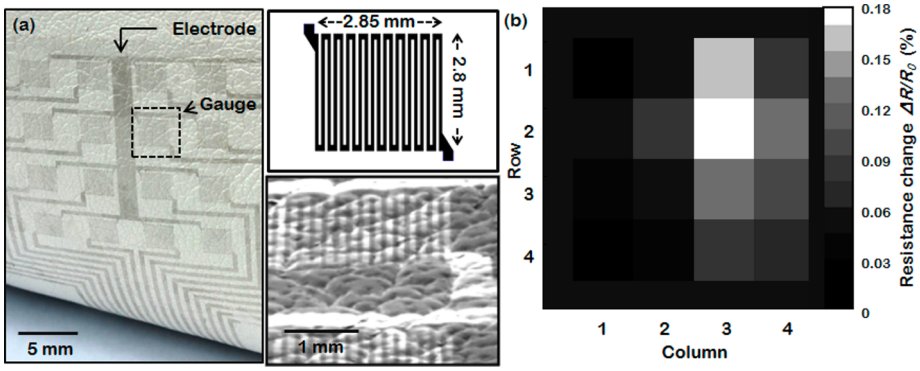


**Figure 6. (a) Photographs of a tactile sensor consisting of ultrathin graphene strain gauges on the animal hide (left), geometric structure of graphene strain gauge (top right), SEM image of graphene strain gauge on animal hide (bottom right). (b) The pressure map measured by the tactile sensor when a gentle touch of 9 kPa was applied to the sensing area.**

basic deformation modes applied by the skin surface as a human body moves (Figure 5(b)). The degrees of bending and twisting in the mechanical tests were set on the basis of the actual hide deformations that occur during elbow bending (Supporting Information, Figure S10). Figure 5(c) showed the mobility variations and endurance cycles of a UT-GFET device in a flat configuration and in a bent or twisted configuration (bending radii: 0.6 cm and twist angle: 25°). The mobility variations were statistically analyzed on 25 randomly selected devices working under identical stresses. As a result, the mobility of the GFETs did not vary significantly regardless of the bending and twisting deformation. Unfortunately, we were not able to calculate the exact stress value of device on hide, because the uneven surface can suppress the applied strain by unfolding the wrinkles; it is carefully estimated that the effective stress applied to the device is not high. Moreover, the devices displayed stable mechanical durability until 130 repeated folding but it showed somewhat vulnerable behavior at twisting deformation (~80 cycles). It is suspected that the partial slip or delamination may occur between transistor and substrate due to sheer force during twisting test, destroying the device. Although the stretchability of the UT-GFETs in conformal contact with the hide was moderate, it could be increased by transferring the as-fabricated device to a more grooved surface.

The presented approach to realize mechanically compliant device is not only useful for transistor application but can be applied for various sensing devices. To demonstrate the feasibility of using this ultrathin, conformable graphene-based device as a tactile sensor, we fabricated a 4 × 4 array with graphene-based resistive strain gauges on an animal hide (Figure 6(a)). The detail fabrication and measurement steps were

described in the Methods section. All device components including strain gauges and electrical lines are composed of monolithically patterned graphene film. The fabricated graphene-based tactile sensor is capable of detecting pressure distribution on the sensing area with a precision better than 9 kPa (Supporting Information, Figure S11) corresponding to the pressure of human's gentle touch as shown in Figure 6(b). The measured gauge factor of each strain gauge was 1.41, which is comparable to the values reported previously.[41,42] This type of the tactile sensor conformably attached on an animal hide could be potentially applicable to the health care monitoring, nonirritating skin-attachable interactive input/control devices and robotics.

## CONCLUSION

In this paper, we demonstrated the conformal devices on an uneven substrate through scaling down the device thickness to 70 nm using atomic-scale graphene and nanometer-thick polymer dielectric as the active and supporting layer of the device, respectively. The graphene-based conformal devices provided excellent conformal coverage over the convoluted surfaces without using an adhesive, due to the extremely low bending stiffness of the device. Consequently, we realized conformal and stretchable devices on animal hide, such as UT-GFET and tactile sensor that have superior conformability to the previous reported results.[4] Moreover, the fabricated devices maintained its original performances well under mechanical bending and twisting. Although the electrical properties of graphene-based conformal devices was moderate (*i.e.*, on/off ratio and gauge factor), it might be possible to be improved by combining other two-dimensional semiconducting materials. The approach presented here to realize the conformal device can offer a key platform for expanding a range of wearable electronic applications such as fitness tracker, smart medical device and health monitoring system.

## METHODS

**SU-8 Epoxy Preparation.** Various thickness of SU-8 layer were used to demmonstrate wearable electronics. To fabricate 70, 220, 430, and 1400 nm thick SU-8 layer, 7, 20, 30, and 60 wt % of mixture were prepared using SU-8 (SU-8 2005, Micro Chemicals) and cyclopetanone (SU-8 2000 thinner, Micro Chemicals). Then the mixture was spin-coated on substrate at 2500 rpm for 30 s. After soft bake the sample at at 65 °C for 5 min, UV exposure was carried out under intensity of 9.3 mJ/cm$^2$ for 2 min. Finally, robust SU-8 films were completed after hard-baking at 150 °C for 30 min.

**Fabrication and Measurement of Bending Stiffness.** To fabricate wavy SU-8 structure, 70, 220, 430, and 1400 nm thick SU-8 layer was prepared on $SiO_2$/Si wafer. Then, we separated the SU-8 film from handling wafer by etching the $SiO_2$ sacrificial layer using diluted HF and rinsed by DI water. At same time, 2 mm thick PDMS slab (Sylgard 184, Dow Corning) was prepared by mixing base and curing agent in a 10:1 weight ratio and back at 70 °C for 2 h. To geneerate wavy SU-8 structure, the PDMS slabe was stretched with mechanical stages before transfer the SU-8 film which was floated on DI-water. When release the strain of PDMS after the SU-8/PDMS sample had dried completely, uniform and regular wavy structure was formed. The wave properties such as wavelenth and amplitue were measured precisely with atomic force microscopy and scanning electron microscope.

**Conformal Tactile Sensor.** The tactile sensor was designed by using only two materials, which are graphene and SU-8 epoxy. First, 35 nm thick SU-8 film was formed on 1 $\mu$m-thick thermal oxide layer ($SiO_2$/Si wafer), and randomly stacked trilayer graphene, which was synthesized using Cu catalyst, was transferred onto SU-8 film. Then the graphene film was monolithically patterned to define strain gauges and electrodes. A typical photolithography process using photoresist (AZ 5214) and reactive ion etching (RIE) with $O_2$ plasma (20 sccm, 100 W, 10 s) was used. Finally, SU-8 epoxy (35 nm) was coated on tactile sensor as a passivation layer. The transfer method used is same as for UT-GFET.

**Measurement of Tactile Sensor.** The tactile sensor was directly connected to the programmable source-meter unit (Keithley 4200-SCS parameter analyzer, Keithley Instruments Inc.) through flexible printed circuit film (MITFPC Inc.). The sensor was measured by using the passive matrix system which has 1 common and 16 data electrodes. After the connection was completed, the pressure was applied to the sensor using home-built pressure arm which had hemisphere-shaped contact part ($r$ = 5 mm) while measuring the weight variation by microelectronic scale. In this time, value of pressure was calculated by the measured weight change and the contact area between pressure arm and sensor.

*Conflict of Interest:* The authors declare no competing financial interest.

*Acknowledgment.* This work was supported by the Research Program (2012R1A2A1A03006049 and Global Frontier Research Center for Advanced Soft Electronics: 2013M3A6A5073170) through the National Research Foundation of Korea (NRF), funded by the Ministry of Science, ICT and Future Planning, and the ICT R & D Program (Grant 10041066) funded by the Institute for Information & Communication Technology Promotion, Korea.

*Supporting Information Available:* Transmittance of ultrathin graphene FET, detail calculation of bending stiffness, Raman spectrum of graphene on animal hide, characterization of conformal graphene FET, and comparison table with previous reported conformal devices. This material is available free of charge *via* the Internet at http://pubs.acs.org.

## REFERENCES AND NOTES

1. Kim, D.-H.; Viventi, J.; Amsden, J. J.; Xiao, J.; Vigeland, L.; Kim, Y. S.; Blanco, J. A.; Panilaitis, B.; Frechette, E. S.; Contreras, D.; *et al.* Dissolvable Films of Silk Fibroin for Ultrathin Conformal Bio-Integrated Electronics. *Nat. Mater.* **2010**, *9*, 511–517.
2. Yeo, W.-H.; Kim, Y. S.; Lee, J.; Ameen, A.; Shi, L.; Li, M.; Wang, S.; Ma, R.; Jin, S. H.; Kang, Z.; *et al.* Multifunctional Epidermal Electronics Printed Directly onto the Skin. *Adv. Mater.* **2013**, *25*, 2773–2778.
3. Webb, R. C.; Bonifas, A. P.; Behnaz, A.; Zhang, Y.; Yu, K. J.; Cheng, H.; Shi, M.; Bian, Z.; Liu, Z.; Kim, Y.-S.; *et al.* Ultrathin Conformal Devices for Precise and Continuous Thermal Characterization of Human Skin. *Nat. Mater.* **2013**, *12*, 938–944.
4. Jeong, J.-W.; Yeo, W.-H.; Akhtar, A.; Norton, J. J.; Kwack, Y. J.; Li, S.; Jung, S. Y.; Su, Y.; Lee, W.; Xia, J.; *et al.* Materials and Optimized Designs for Human-Machine Interfaces *via* Epidermal Electronics. *Adv. Mater.* **2013**, *25*, 6839–6846.
5. Sekitani, T.; Nakajima, H.; Maeda, H.; Fukushima, T.; Aida, T.; Hata, K.; Someya, T. Stretchable Active-Matrix Organic

Light-Emitting Diode Display Using Printable Elastic Conductors. *Nat. Mater.* **2009**, *8*, 494–499.
6. Vosgueritchian, M.; Tok, J. B. H.; Bao, Z. N. Stretchable LEDs: Light-Emitting Electronic Skin. *Nat. Photonics* **2013**, *7*, 769–771.
7. Chun, K.-Y.; Oh, Y.; Rho, J.; Ahn, J.-H.; Kim, Y.-J.; Choi, H. R.; Baik, S. Highly Conductive, Printable and Stretchable Composite Films of Carbon Nanotubes and Silver. *Nat. Nanotechnol.* **2010**, *5*, 853–857.
8. Someya, T.; Kato, Y.; Sekitani, T.; Iba, S.; Noguchi, Y.; Murase, Y.; Kawaguchi, H.; Sakurai, T. Conformable, Flexible, Large-Area Networks of Pressure and Thermal Sensors with Organic Transistor Active Matrixes. *P. Natl. Acad. Sci. U. S. A.* **2005**, *102*, 12321–12325.
9. Takahashi, T.; Takei, K.; Gillies, A. G.; Fearing, R. S.; Javey, A. Carbon Nanotube Active-Matrix Backplanes for Conformal Electronics and Sensors. *Nano Lett.* **2011**, *11*, 5408–5413.
10. Lacour, S. P.; Chan, D.; Wagner, S.; Li, T.; Suo, Z. G. Mechanisms of Reversible Stretchability of Thin Metal Films on Elastomeric Substrates. *Appl. Phys. Lett.* **2006**, *88*, 204103.
11. Hung, P. J.; Jeong, K. H.; Liu, G. L.; Lee, L. P. Microfabricated Suspensions for Electrical Connections on the Tunable Elastomer Membrane. *Appl. Phys. Lett.* **2004**, *85*, 6051–6053.
12. Ko, H. C.; Shin, G.; Wang, S. D.; Stoykovich, M. P.; Lee, J. W.; Kim, D.-H.; Ha, J. S.; Huang, Y. G.; Hwang, K.-C.; Rogers, J. A. Curvilinear Electronics Formed Using Silicon Membrane Circuits and Elastomeric Transfer Elements. *Small* **2009**, *5*, 2703–2709.
13. Kim, D.-H.; Kim, Y. S.; Wu, J.; Liu, Z. J.; Song, J. Z.; Kim, H.-S.; Huang, Y. G. Y.; Hwang, K. C.; Rogers, J. A. Ultrathin Silicon Circuits With Strain-Isolation Layers and Mesh Layouts for High-Performance Electronics on Fabric, Vinyl, Leather, and Paper. *Adv. Mater.* **2009**, *21*, 3703–3707.
14. Kim, D.-H.; Choi, W. M.; Ahn, J.-H.; Kim, H.-S.; Song, J. Z.; Huang, Y. G.; Liu, Z. J.; Lu, C.; Koh, C. G.; Rogers, J. A. Complementary Metal Oxide Silicon Integrated Circuits Incorporating Monolithically Integrated Stretchable Wavy Interconnects. *Appl. Phys. Lett.* **2008**, *93*, 044102.
15. Kim, D.-H.; Song, J. Z.; Choi, W. M.; Kim, H.-S.; Kim, R.-H.; Liu, Z. J.; Huang, Y. Y.; Hwang, K.-C.; Zhang, Y. W.; Rogers, J. A. Materials and Noncoplanar Mesh Designs for Integrated Circuits with Linear Elastic Responses to Extreme Mechanical Deformations. *P. Natl. Acad. Sci. U. S. A.* **2008**, *105*, 18675–18680.
16. Song, Y. M.; Xie, Y. Z.; Malyarchuk, V.; Xiao, J. L.; Jung, I.; Choi, K.-J.; Liu, Z. J.; Park, H.; Lu, C. F.; Kim, R. H.; *et al.* Digital Cameras With Designs Inspired by the Arthropod Eye. *Nature* **2013**, *497*, 95–99.
17. Park, K.; Lee, D.-K.; Kim, B.-S.; Jeon, H.; Lee, N.-E.; Whang, D.; Lee, H.-J.; Kim, Y. J.; Ahn, J.-H. Stretchable, Transparent Zinc Oxide Thin Film Transistors. *Adv. Funct. Mater.* **2010**, *20*, 3577–3582.
18. Kaltenbrunner, M.; White, M. S.; Glowacki, E. D.; Sekitani, T.; Someya, T.; Sariciftci, N. S.; Bauer, S. Ultrathin and Lightweight Organic Solar Cells with High Flexibility. *Nat. Commun.* **2012**, *3*, 770.
19. Viventi, J.; Kim, D.-H.; Moss, J. D.; Kim, Y.-S.; Blanco, J. A.; Annetta, N.; Hicks, A.; Xiao, J. L.; Huang, Y. G.; Callans, D. J.; *et al.* A Conformal, Bio-Interfaced Class of Silicon Electronics for Mapping Cardiac Electrophysiology. *Sci. Transl. Med.* **2010**, *2*, 22–24.
20. Kim, D.-H.; Lu, N. S.; Ma, R.; Kim, Y. S.; Kim, R.-H.; Wang, S. D.; Wu, J.; Won, S. M.; Tao, H.; Islam, A.; *et al.* Epidermal Electronics. *Science* **2011**, *333*, 838–843.
21. Lee, S.-K.; Kim, B. J.; Jang, H.; Yoon, S. C.; Lee, C.; Hong, B. H.; Rogers, J. A.; Cho, J. H.; Ahn, J.-H. Stretchable Graphene Transistors with Printed Dielectrics and Gate Electrodes. *Nano Lett.* **2011**, *11*, 4642–4646.
22. Lee, S.-K.; Jang, H. Y.; Jang, S.; Choi, E.; Hong, B. H.; Lee, J.; Park, S.; Ahn, J.-H. All Graphene-Based Thin Film Transistors on Flexible Plastic Substrates. *Nano Lett.* **2012**, *12*, 3472–3476.
23. Lee, K.; Park, J.; Lee, M.-S.; Kim, J.; Hyun, B. G.; Kang, D. J.; Na, K.; Lee, C. Y.; Bien, F.; Park, J.-U. *In-Situ* Synthesis of Carbon Nanotube-Graphite Electronic Devices and Their Integrations onto Surfaces of Live Plants and Insects. *Nano Lett.* **2014**, *14*, 2647–2654.
24. Lee, M.-S.; Lee, K.; Kim, S.-Y.; Lee, H.; Park, J.; Choi, K.-H.; Kim, H.-K.; Kim, D.-G.; Lee, D.-Y.; Nam, S.; *et al.* High-Performance, Transparent, and Stretchable Electrodes Using Graphene-Metal Nanowire Hybrid Structures. *Nano Lett.* **2013**, *13*, 2814–2821.
25. Jang, H.; Lee, W.; Won, S. M.; Ryu, S. Y.; Lee, D.; Koo, J. B.; Ahn, S.-D.; Yang, C.-W.; Jo, M. H.; Cho, J. H.; *et al.* Quantum Confinement Effects in Transferrable Silicon Nanomembranes and Their Applications on Unusual Substrates. *Nano Lett.* **2013**, *13*, 5600–5607.
26. O'Connor, T. F.; Zaretski, A. V.; Shiravi, B. A.; Savagatrup, S.; Printz, A. D.; Diaz, M. I.; Lipomi, D. J. Stretching and Conformal Bonding of Organic Solar Cells to Hemispherical Surfaces. *Energy Environ. Sci.* **2014**, *7*, 370–378.
27. Kim, K. S.; Zhao, Y.; Jang, H.; Lee, S. Y.; Kim, J. M.; Kim, K. S.; Ahn, J.-H.; Kim, P.; Choi, J. Y.; Hong, B. H. Large-Scale Pattern Growth of Graphene Films for Stretchable Transparent Electrodes. *Nature* **2009**, *457*, 706–710.
28. Cao, Q.; Xia, M. G.; Shim, M.; Rogers, J. A. Bilayer Organic-Inorganic Gate Dielectrics for High-Performance, Low-Voltage, Single-Walled Carbon Nanotube Thin-Film Transistors, Complementary Logic Gates, and P-N Diodes on Plastic Substrates. *Adv. Funct. Mater.* **2006**, *16*, 2355–2362.
29. Li, X. S.; Cai, W. W.; An, J. H.; Kim, S.; Nah, J.; Yang, D. X.; Piner, R.; Velamakanni, A.; Jung, I.; Tutuc, E.; *et al.* Large-Area Synthesis of High-Quality and Uniform Graphene Films on Copper Foils. *Science* **2009**, *324*, 1312–1314.
30. Bae, S.; Kim, H.; Lee, Y.; Xu, X. F.; Park, J.-S.; Zheng, Y.; Balakrishnan, J.; Lei, T.; Kim, H. R.; Song, Y. I.; *et al.* Roll-to-Roll Production of 30-Inch Graphene Films for Transparent Electrodes. *Nat. Nanotechnol.* **2010**, *5*, 574–578.
31. Thanh, Q. N.; Jeong, H.; Kim, J.; Kevek, J. W.; Ahn, Y. H.; Lee, S.; Minot, E. D.; Park, J. Y. Transfer-Printing of As-Fabricated Carbon Nanotube Devices onto Various Substrates. *Adv. Mater.* **2012**, *24*, 4499–4504.
32. Park, J.-U.; Nam, S.; Lee, M.-S.; Lieber, C. M. Synthesis of Monolithic Graphene-Graphite Integrated Electronics. *Nat. Mater.* **2012**, *11*, 120–125.
33. Chaudhury, M. K.; Whitesides, G. M. Direct Measurement of Interfacial Interactions between Semispherical Lenses and Flat Sheets of Poly(dimethylsiloxane) and Their Chemical Derivatives. *Langmuir* **1991**, *7*, 1013–1025.
34. Persson, B. N. J.; Tosatti, E. The Effect of Surface Roughness on the Adhesion of Elastic Solids. *J. Chem. Phys.* **2001**, *115*, 5597–5610.
35. Persson, B. N. J.; Albohr, O.; Creton, C.; Peveri, V. Contact Area between a Viscoelastic Solid and a Hard, Randomly Rough, Substrate. *J. Chem. Phys.* **2004**, *120*, 8779–8793.
36. Palasantzas, G.; De Hosson, J. T. M. Influence of Surface Roughness on the Adhesion of Elastic Films. *Phys. Rev. E: Stat., Nonlinear, Soft Matter Phys.* **2003**, *67*, 021604.
37. Varenberg, M.; Peressadko, A.; Gorb, S.; Arzt, E. Effect of Real Contact Geometry on Adhesion. *Appl. Phys. Lett.* **2006**, *89*, 121905.
38. Suo, Z.; Ma, E. Y.; Gleskova, H.; Wagner, S. Mechanics of Rollable and Foldable Film-on-Foil Electronics. *Appl. Phys. Lett.* **1999**, *74*, 1177–1179.
39. Lee, G. H.; Cooper, R. C.; An, S. J.; Lee, S.; van der Zande, A.; Petrone, N.; Hammerherg, A. G.; Lee, C.; Crawford, B.; Oliver, W.; *et al.* High-Strength Chemical-Vapor Deposited Graphene and Grain Boundaries. *Science* **2013**, *340*, 1073–1076.
40. Ni, G.-X.; Yang, H.-Z.; Ji, W.; Baeck, S.-J.; Toh, C. T.; Ahn, J.-H.; Pereira, V. M.; Ozyilmaz, B. Tuning Optical Conductivity of Large-Scale CVD Graphene by Strain Engineering. *Adv. Mater.* **2014**, *26*, 1081–1086.
41. Chang, L. *Foundations of MEMS*; Pearson Education: Cranbury Township, NJ, 2006; pp 207–244.
42. Huang, M.; Pascal, T. A.; Kim, H.; Goddard, W. A., III; Greer, J. R. Electronic-Mechanical Coupling in Graphene from *In-Situ* Indentation Experiments and Multiscale Simulations. *Nano Lett.* **2011**, *11*, 1241–1246.